DOI: 10.31276/VJSTE.2025.0078

Experimental and numerical study on the influence of explosive charge length on the performance of explosively formed projectiles

Hong Quan Pham*, Van Minh Do, Dinh Thanh Tran

Le Quy Don Technical University, 236 Hoang Quoc Viet Street, Nghia Do Ward, Hanoi, Vietnam

Received 28 September 2025; revised 9 October 2025; accepted 5 December 2025

Abstract:

Understanding how the length of the explosive charge affects the formation and terminal performance of explosively formed projectiles (EFPs) is crucial for designing efficient warheads. In this study, eleven EFP configurations with charge lengths ranging from 0.7 to 1.7 times the liner diameter were analysed using high-fidelity ANSYS Autodyn simulations. An experimental test with l/*d*=1.2 was conducted to validate the simulation. The results show that projectile velocity, penetration depth, and penetration diameter all increase with charge length up to 1.2-1.4*d*, beyond which performance plateaus. The experimental velocity deviated by less than 2.3% and the penetration diameter by less than 5.7%, indicating that the proposed model agrees well with the experimental results. These findings provide practical guidance for optimising EFP warhead design.

***Keywords*:** **ANSYS Autodyn, charge length, explosively formed projectile, numerical simulation, penetration depth.**

**Corresponding author: Email: phquanstudying@lqdtu.edu.vn*

Classification number: **2.3.**

1. Introduction

Explosively formed projectiles (EFPs), also known as self-forming fragments, are a type of advanced weapon designed to penetrate armour at high speeds and over long distances. A conventional EFP warhead comprises a ductile metallic liner-typically hemispherical and fabricated from oxygen-free high-conductivity (OFHC) copper-surrounded by a high explosive charge and encased within a containment shell. Upon detonation, intense shock waves and detonation gases exert high-pressure loading on the liner, inducing a rapid collapse that reshapes it into a coherent, high-speed projectile. These projectiles can attain velocities ranging from 1500 to 2500 m/s, with the capability to perforate armour plates up to one calibre thick, depending on the charge geometry and stand-off distance [1, 2]. The performance and aerodynamic stability of the formed projectile are critically governed by the detonation velocity and the spatial configuration of the explosive, making them essential design parameters in EFP warhead development.

Numerous domestic and international studies have investigated the effects of material properties, geometrical parameters and explosive types on EFP formation. J. Wu, et al. (2007) [3] proposed a preliminary structure of the liner and explosive charge. D.V. Minh, et al. (2025) [4] investigated the effect of the liner curvature radius on EFP velocity and penetration using numerical simulation, reporting discrepancies of less than 8% when compared with experimental results. H.Q. Pham, et al. (2025) [5] studied the effect of the liner height and found that a liner height of 0.2-0.3 times the liner diameter produced EFPs with good aerodynamic shape, achieving high velocity and large penetration depth. O. Jeremić, et al. (2017) [6] evaluated discrepancies between numerical simulations and analytical methods for liner performance, reporting deviations of less than 13%. H. Couque, et al. (2006), (2007), G. Hussain, et al. (2013) [7-9] conducted experiments and recommended the use of ANSYS Autodyn software with a modified Johnson-Cook (KJC) model to achieve smaller errors compared to the Johnson-Cook (JC) model. W. Li et al. [10] conducted combined numerical and experimental studies to evaluate the impact of explosive charge length on EFP performance. They reported a significant 74.5% increase in projectile velocity when the charge length was increased from 0.9 to 1.4 times the charge diameter, while further extension to 1.6 diameters yielded only a marginal 1.9% gain. S.M. Zakir, et al. (2018) [11] demonstrated that optimising the length-to-diameter ratio within the range of 0.75-1.1 can lead to the formation of either high-velocity or elongated EFPs, depending on the liner configuration [11]. M. Petrudi, et al. [12] performed numerical and analytical simulations of ballistic projectile penetration due to high-velocity impact on ceramic targets. Furthermore, M. Rahmani, et al. (2020) [13] also conducted experimental and numerical optimisation studies of shock wave damping in aluminium panel sandwich structures.

This study develops a mathematical model of explosive loading and element deformation and employs numerical simulation to study EFP formation and its interaction with steel targets. Simulation results are presented for configurations with varying explosive charge lengths to investigate their effect on projectile formation and penetration behaviour. Based on these results, recommendations for optimal charge length in EFP design are derived. Experimental tests were also conducted for a selected configuration to validate the numerical model and to quantify discrepancies between experimental and simulated outcomes.

2. Materials and methods

2.1. Geometric model and calculation method

The study focuses on a 54 mm EFP warhead, shown in Fig. 1. The warhead includes four main components: the casing, explosive charge, detonator, and liner. The liner, made of oxygen-free highconductivity (OFHC) copper, has a hemispherical profile characterised by its height *h*, diameter *d*, outer radius r_1, and inner radius r_2. The liner also includes a top thickness δ_1, an edge thickness δ_2, and two geometric offsets X_1 and X_2, which represent the distances from the centres of the outer and inner radii, respectively, to the bottom of the warhead along the axis of symmetry (OX).

The casing, constructed from polyethylene plastic, is designed as a cylindrical shell with an outer diameter *D*, total length *L*, wall thickness t_1 for the cylindrical section, and a bottom thickness t_2. The explosive filler, C4, was placed inside the casing and specified by diameter *d* and height *l*. Initiation was provided by a 4 mm × 4 mm electric detonator.

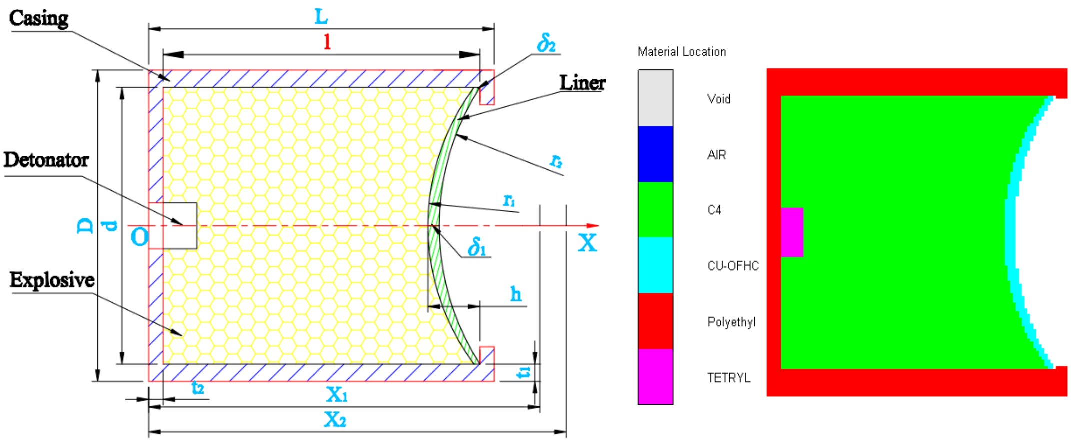

Fig 1. EFP model and simulation model in ANSYS Autodyn.

To establish the structural parameters of the warhead model under investigation, it was necessary to define not only the calibre of the device *D* and the diameter of the explosive charge *d*, but also a set of preliminary design inputs. In accordance with the recommendations presented in references [5], the liner thickness was specified to vary gradually from the top to the edge in order to ensure optimised deformation characteristics. The explosive material selected for this study was C4, encased within a polyethylene shell to replicate typical field configurations. Previous studies [10, 11] have reported that effective charge lengths typically range from 0.75 to 1.6 times the calibre. Based on this guidance, the present study considered a broader interval, ranging from 0.7 to 1.7 times the diameter of the explosive charge (*d*), to comprehensively evaluate performance trends. The specific geometric and structural parameters corresponding to each design configuration are summarised in Table 1.

Table 1. Parameters of EFPW with different explosive charge lengths.

Pa.	**Unit**	**Type**										
		1	**2**	**3**	**4**	**5**	**6**	**7**	**8**	**9**	**10**	**11**
D	mm	54										
d	mm	45.2										
δ_1	mm	1										
δ_2	mm	2										
t_1	mm	4.4										
t_2	mm	2.5										
h	mm	9.04										
r_1	mm	35.78										
r_2	mm	39.8										
l	mm	31.64	36.16	40.68	45.2	49.72	54.24	58.76	63.28	67.8	72.32	76.84
L	mm	36.64	41.16	45.68	50.2	54.72	59.24	63.76	68.28	72.8	77.32	81.84
X_1	mm	60.88	65.4	69.92	74.44	78.96	83.48	88	92.52	97.04	101.56	106.08
X_2	mm	66.99	71.51	76.03	80.55	85.07	89.59	94.11	98.63	103.15	107.67	112.19
l/d		0.7	0.8	0.9	1	1.1	1.2	1.3	1.4	1.5	1.6	1.7

The formation of the EFP and its interaction with steel targets were simulated using ANSYS Autodyn. The output parameters obtained from the EFP formation stage were subsequently used as input data for modelling its impact on steel plates. To exploit axial symmetry and reduce computational cost, the problem was modelled as a two-dimensional axisymmetric case. The casing, liner, explosive, and surrounding air were represented on the Eulerian grid with a cell size of 0.25

mm × 0.25 mm. Flow-out boundary conditions were applied to all domain boundaries except along the axis of symmetry. The complete geometric setup, including element selection, mesh generation, geometry creation, material assignment, and gauge placement, was implemented within the Autodyn-2D environment [7, 10, 11, 14].

2.2. Material model and parameters

The plastic explosive C4 was modelled as an ideal elastoplastic material governed by the von Mises yield criterion. Upon detonation, C4 undergoes a rapid phase transition into gaseous products, which were characterised using the Jones-Wilkins-Lee (JWL) equation of state. In this formulation, the detonation product pressure p is expressed as a function of the relative volume V and the specific internal energy E, allowing accurate representation of the expansion behaviour of the detonation gases.

$$p = A\left(1-\frac{\omega}{R_1 V}\right)e^{-R_1 V} + B\left(1-\frac{\omega}{R_2 V}\right)e^{-R_2 V} + \frac{\omega E}{V} \quad (1)$$

where ω, A, B, R_1 and R_2 are material constants obtained experimentally. The values of these constants used in the present study are listed in Table 2. This model enables accurate representation of the pressure-volume-energy relationship of detonation products and ensures reliable prediction of EFP formation dynamics [7-9].

Table 2. Values of the parameters in the JWL equation for the state of C4 explosive.

ω	A, GPa	B, GPa	R_1	R_2	ρ, g/cm^3	E, J/m^3
0.25	0.60977	0.01295	4.5	1.4	1.601	9×10^9

The casing of the warhead was modelled using polyethylene plastic. Under explosive loading, the material undergoes large volumetric compression and significant shape deformation. To capture this response, the shock equation of state (EOS) was employed. The parameters in the model are experimentally determined constants, and their specific values are provided in Table 3. This approach ensures accurate representation of the casing's dynamic behaviour during detonation and subsequent EFP formation [13].

$$U_s = C_1 + S_1 u_p \tag{2}$$

$$P(\rho, e) = P_H(\rho) + \rho\Gamma(e - e_H(\rho)) \tag{3}$$

where u_p is particle velocity, e is the specific internal energy, Γ is the Grüneisen coefficient, P_H and e_H are the pressure and internal energy on the Hugoniot curve, respectively.

Table 3. Values of the parameters in the Shock equation for the polyethylene plastic.

ρ, g/cm^3	Γ	C_1, cm/μs	S_1	C_2, cm/μs	S_2	$\frac{VE}{v_o}$	$\frac{VB}{v_o}$
0.915	1.64	0.2901	1.481	0	0	0	0

The liner is usually made of red copper M1 described by the modified Johnson-Cook (KJC) elastic-plastic model [7-9].

$$\sigma = \left(A + B\varepsilon_p{}^n\right)\left(1 + C\ln\left(\frac{\varepsilon^*}{\varepsilon^*_\bullet}\right) + D\left(\frac{\varepsilon^*}{\varepsilon^*_l}\right)^k\right)\left(1 - T_A^m\right) \tag{4}$$

where σ is the dynamic yield stress; A, B, C, D, n, m and k are the constants of the material determined experimentally; ε_p is the plastic strain; ε^* - is the plastic strain rate; $\varepsilon^*_\bullet$ is the reference value for plastic strain rate; ε^*_l is the reference strain rate characterising the transition between thermally activated and viscous regime; $T_A = \frac{T - T_{ref}}{T_{melt} - T_{ref}}$; T is the instantaneous temperature; T_{ref} is the initial temperature; and T_{melt} is the melting temperature of the material. In this simulation, the liner was composed of oxygen-free high-conductivity copper (Cu-OFHC) and modelled using the Modified Johnson-Cook (KJC) constitutive model. To suppress plastic instability under high strain-rate conditions (10^3-10^6) s^{-1}, the hardening constant was increased by 10%, from 29.2 GPa to 32.1 GPa. The target plate was made of Steel 1006 and represented using the standard Johnson-Cook (JC) model. The corresponding material parameters for both models are summarised in Table 4. These constitutive descriptions ensure accurate simulation of liner deformation, projectile formation, and target response under extreme loading conditions [7-9].

Table 4. Parameter values in the elastic-plastic model.

Parameters	**Unit**	**Value**	
		CU-OFHC	***Steel 1006***
Equation of state	-	Linear	Shock
Density	kg/m^3	8960	7 830
Melting temperature	K	1356	1811
Strength model	-	JC	JC
Yield stress A	Gpa	0.09	0.35
Hardening constant B	Gpa	0.3212	0.275
Strain rate constant C	-	0.025	0.022
Hardening exponent n	-	0.31	0.36
Thermal softening exponent m	-	1.09	1

In the numerical simulation, the equation of state (EOS) of air was represented using the gamma-law form, which provides a simple yet effective description of the pressure-density-energy relationship for gases [15].

$$p = \rho(\gamma - 1)E \tag{5}$$

where γ =1.4; ρ=1.225 kg/m^3, and E =2.5×10^5 J/kg.

During the penetration phase, a Lagrangian mesh was employed for both the EFP and the target. The projectile parameters obtained from the Eulerian simulation of the formation process were used as input conditions for the penetration analysis. The target material was modelled as a steel plate (Steel 1006) with dimensions of 200 mm in width and 30 mm in thickness. Its thermodynamic behaviour was described using the shock equation of state, while the mechanical response and failure characteristics were represented by the Johnson-Cook constitutive and damage models [15].

$$D_* = \sum \frac{\Delta\varepsilon}{\varepsilon^f} \tag{6}$$

$$\varepsilon^f = \left[D_1 + D_2 e^{D_3\sigma^*}\right]\left[1 + D_4 \ln \dot{\varepsilon}_*\right]\left[1 + D_5 T_A\right] \tag{7}$$

where D_1, D_2, D_3, D_4, D_5 are failure parameters, ε^f is the equivalent strain to failure, $\dot{\varepsilon}_*$ is the non-dimensional strain rate, and σ^* is the stress triaxiality

Table 5. Values of Johnson-Cook failure model parameters.

D_1	D_2	D_3	D_4	D_5
0.05	4.22	-2.73	0.0018	0.55

The simulation model of the EFP impact on the steel target is illustrated in Fig. 2. Both the projectile and the target were discretised using rectangular elements with a uniform mesh size of 0.25 mm [5,16].

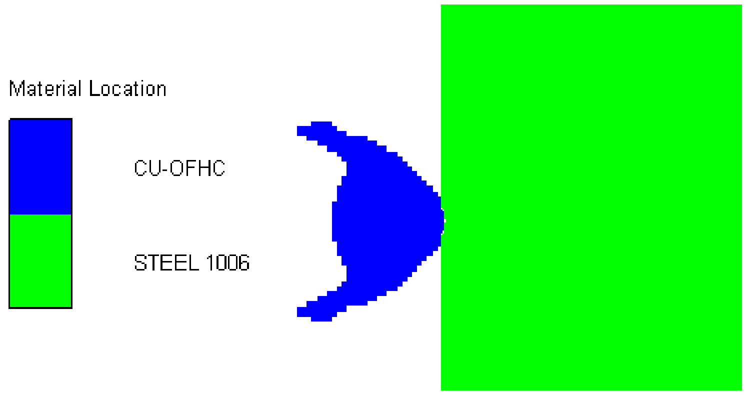

Fig. 2. Simulation of EFP impact on steel plate.

3. Simulation model and material model

3.1. Explosively formed projectiles and experimental target

For experimental validation, the liner with structure type 2 was selected, with its geometry and dimensions summarised in Table 1. The liner material was M1 copper, while the casing was made of polyethylene plastic. The explosive charge consisted of C4 plastic explosive, initiated by a No. 8 electric detonator. The target material was 45# steel, fabricated into a square plate with dimensions of 500 mm×500 mm and a thickness of 20 mm, as shown in Fig. 3.

Fig. 3. EFP and steel target.

3.2. Experimental setup

To validate the numerical model under representative conditions, an experimental test was conducted using a warhead with a charge length of 54.24 mm (*l/d*=1.2), selected based on the optimal range identified in the simulation. As illustrated in Fig. 4, the EFP warhead was mounted horizontally, with a 20 mm-thick 45# steel plate positioned 3 m downstream to serve as the target. An electronic timer (UTC-8), placed 2 m from the warhead, was used to record the projectile velocity. Following impact, the diameter and depth of the penetration hole in the target plate were measured to evaluate the EFP's terminal performance and to compare it with the simulated results for Type 6.

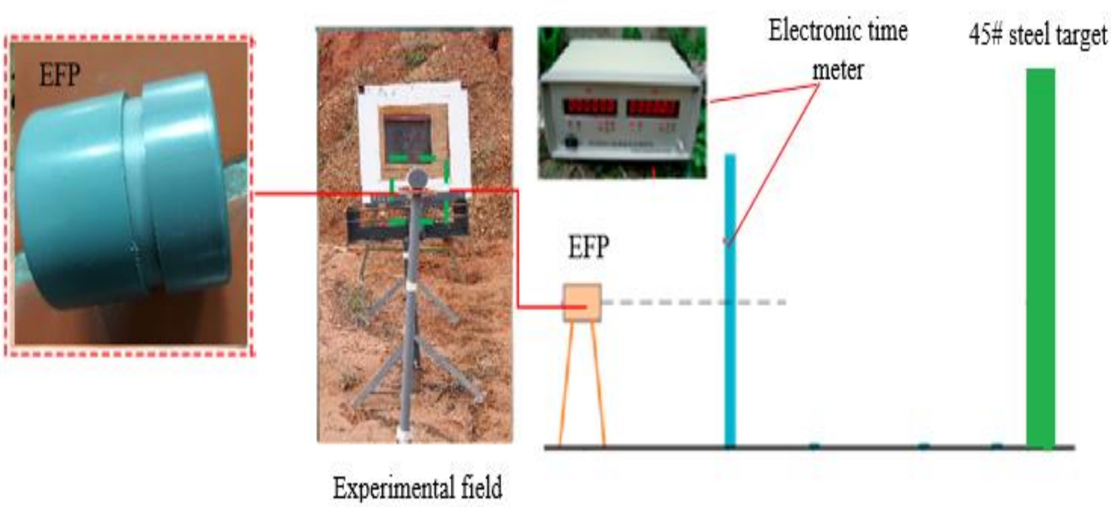

Fig. 4. Experimental measurement of EFP velocity and penetration depth.

3.3. Experimental results

After the static blasting of the test specimens, the dimensions of the through hole on the steel plate were measured to determine its diameter and depth, as shown in Fig. 5.

Symbol 0.1 Symbol 0.2 Symbol 0.3

Fig. 5. Experimental results of EFP interaction with steel plate.

The results of EFP velocity *V*, penetration diameter *b*, and penetration depth d_h when tested for each type of EFP are shown in Table 6.

Table 6. EFP velocity and penetration results on steel target.

Type with *l/d*=1.2			
Symbol	0.1	0.2	0.3
V(m/s)	2278	2150	1859
V_{Avg} (m/s)	2096		
b (mm)	36	37	40
b_{Avg} (mm)	37.7		
d_h (mm)	> 20	> 20	18

4. Discussion

Table 7 presents the results of the investigation on the impact of length explosive on EFP formation in EFPW at time *t*=0.5 m/s for all EFP warhead structures with the parameters listed in Table 1.

4.1. Shape of EFP

The simulation results in Table 7 show that the shape of the explosively formed projectile (EFP) depends strongly on the length of the explosive charge. During the early stage of formation (*t*=0.05-0.15 m/s), the liner expands radially and begins to collapse. As the collapse continues (*t*=0.35-0.5 m/s), the liner transforms into a streamlined, forward-facing projectile with good aerodynamic stability [2].

For charge lengths of 0.7*d*-1.1*d* (Types 1-5), the liner collapse is incomplete, producing short projectiles with less efficient formation. At 1.2*d* (Type 6), the liner fully collapses, forming a longer and sharper EFP, which indicates stronger axial convergence and improved energy transfer. When the charge length exceeds

1.4*d* (Types 9-11), the projectile shape no longer changes significantly, and the maximum displacement stabilises around 1146 mm. This indicates that adding more explosive material does not further improve the projectile shape, marking the onset of geometric saturation.

In summary, the optimal charge length lies in the range of 1.2*d*-1.4*d*, which yields EFPs with stable, aerodynamic shapes, thereby ensuring improved flight performance and penetration capability.

4.2. Velocity of EFP

The simulation results demonstrate a clear relationship between the length of the explosive charge and the velocity of the EFP. As the charge length increased from 0.7 to 1.4 times the liner diameter (corresponding to configurations Type 1 to Type 8), the velocity of the EFP steadily increased from 1962 m/s to 2157 m/s. The most substantial gains were observed between configurations Type 1 and Type 6, with an average increase of approximately 36.4 m/s per configuration. However, beyond Type 8 (1.4 times the liner diameter), further increases in charge length yielded no additional velocity gains. From Type 8 through Type 11 (up to 1.7 times the charge diameter), the velocity remained constant at 2157 m/s. This trend indicates a performance plateau, beyond which the added explosive mass does not enhance the projectile's kinetic energy [17-19].

Table 7. Shape of EFP at specific times and displacements.

Time (ms)		**0.05**	**0.15**	**0.35**	**0.5**
Type 1 V_{EFP} =1962 m/s E_{kin}=39.15 kJ	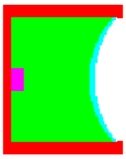				
	Displacement (mm)	145	343	738	1068

Type 2 V_{EFP} =2026 m/s E_{kin}=40.79 kJ	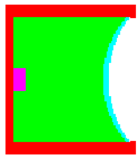	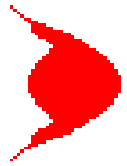	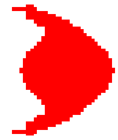	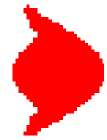	
	Displacement (mm)	165	370	799	1084
Type 3 V_{EFP} =2074 m/s E_{kin}=42.85 kJ	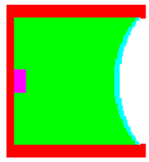	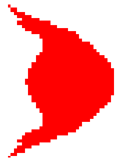	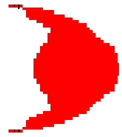		
	Displacement (mm)	167	377	795	1107
Type 4 V_{EFP} =2110 m/s E_{kin}=44.56 kJ	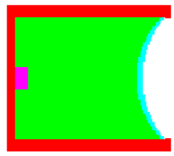				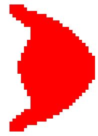
	Displacement (mm)	169	381	806	1112
Type 5 V_{EFP} =2129 m/s E_{kin}=45.23 kJ	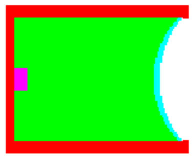				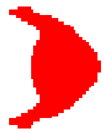
	Displacement (mm)	170	384	811	1131
Type 6 V_{EFP} = 2144 m/s E_{kin}= 45.63 kJ	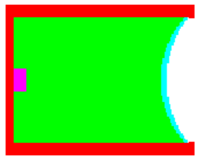	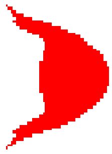	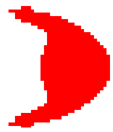	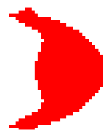	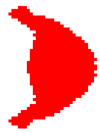
	Displacement (mm)	171	386	817	1140
Type 7 V_{EFP} = 2154 m/s E_{kin}= 45.81 kJ	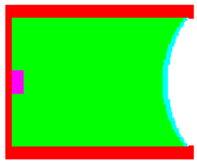	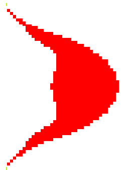	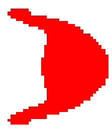		
	Displacement (mm)	171	387	820	1142

Type 8 V_{EFP} = 2157 m/s E_{kin}= 45.91 kJ	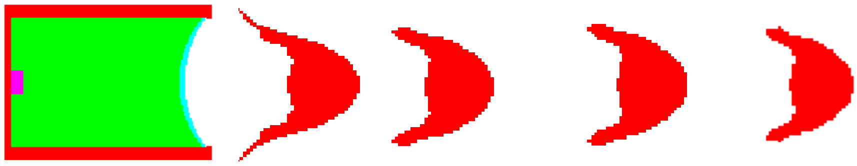				
	Displacement (mm)	171	388	822	1146
Type 9 V_{EFP} = 2157 m/s E_{kin}= 45.92 kJ	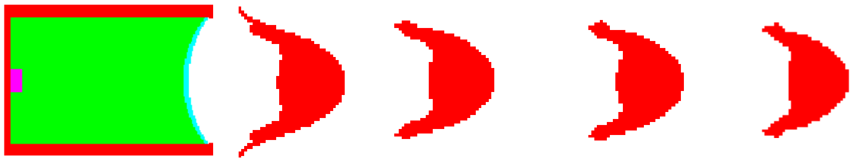				
	Displacement (mm)	171	388	822	1146
Type 10 V_{EFP} =2157 m/s E_{kin}=45.93 kJ	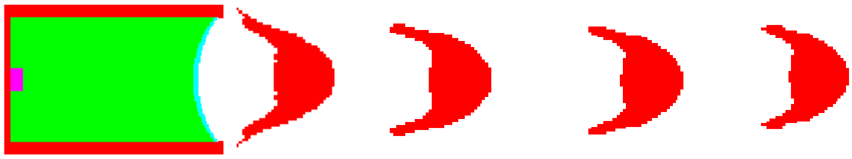				
	Displacement (mm)	171	388	822	1146
Type 11 V_{EFP} =2157 m/s E_{kin}=45.96 kJ					
	Displacement (mm)	171	388	822	1146

Based on the results obtained from the experiment on the Type 6 with *l/d*=1.2, the velocities of the three test specimens were 2278 m/s, 2150 m/s, and 1859 m/s, respectively. The average EFP velocity of the three specimens was 2096 m/s, with a 2.2% deviation compared to the simulation results. The difference between the simulation and experimental results was less than 15%, which is within the allowable range.

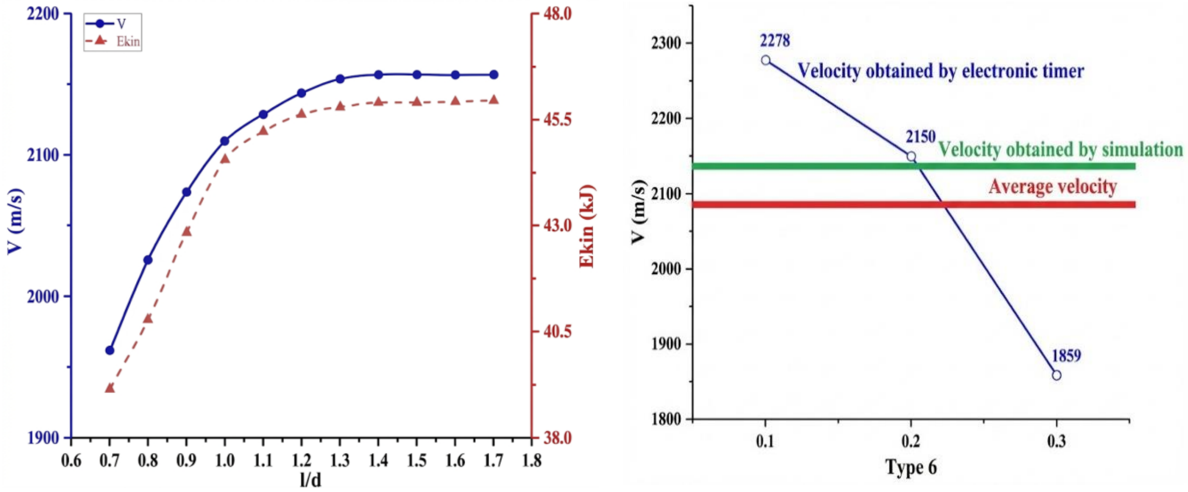

Fig. 6. Velocity of EFP obtained by simulation and experiments.

4.3. Kinetic energy of EFP

Data in Table 7 show that the kinetic energy of the EFP increases markedly with charge length in the range of *l/d*=0.7 to 1.1, consistent with improvements in both velocity and projectile mass. The energy peaks within the range *l/d*=1.2-1.4, indicating an optimal balance between axial acceleration and liner deformation. Beyond this range, the growth in kinetic energy diminishes, revealing a saturation effect in which added explosive mass contributes little to further performance. This trend underscores the importance of selecting charge lengths that maximise energy transfer efficiency. Maintaining *l/d* within the 1.2-1.4 interval offers the most effective use of explosive material while ensuring high terminal performance.

4.4. Penetration process

Following formation, the EFP impacts a 45# steel target plate with a thickness of 30 mm. As illustrated in Fig. 4, the target material experiences significant compressive and shear stresses, which constitute the primary failure mechanisms during interaction with the EFP. A combined tensile-compressive stress distribution is observed at both the front and rear surfaces of the target. As penetration progresses, tensile stresses increasingly dominate, particularly at the edges of the shear zone, due to pronounced material elongation. The reflection of transverse waves at the rear surface, along with continuous projectile penetration, further accelerates target degradation.

Two distinct active zones are identified: a compressive zone near the front surface, where compressive failure prevails, and a tensile zone near the rear surface, characterised by tensile-induced damage. The penetration depth was determined by measuring the through-hole created in a standardised steel plate after impact. With increasing penetration depth, resistance to projectile motion intensifies, resulting in an expanding damage region within the target.

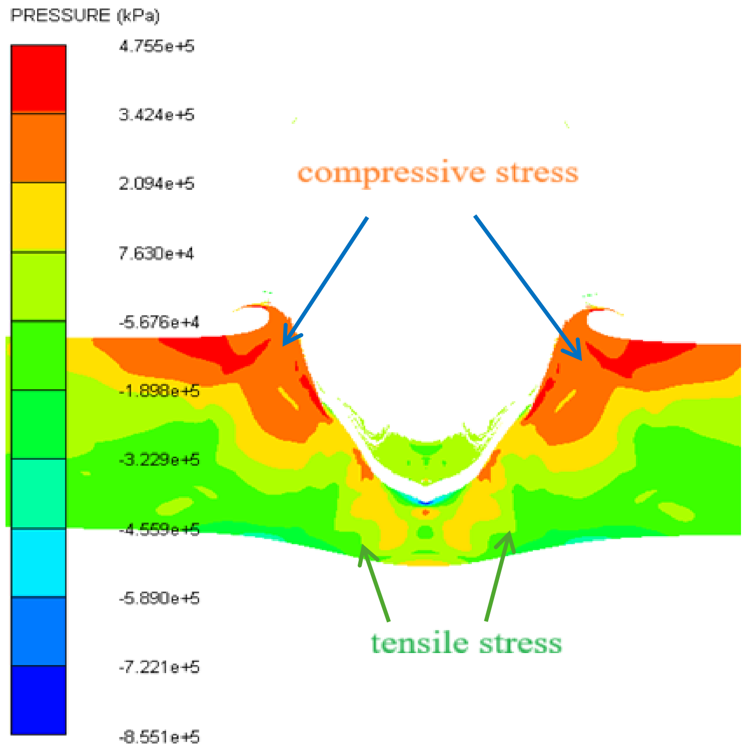

Fig. 7. Steel target plate subjected to EFP impact.

In the shorter configurations (Types 1-4), the penetration depth increases from 22 mm to 25 mm, while the penetration diameter decreases from 41 mm to

39 mm. This implies that a longer explosive charge produces a more slender projectile, focusing energy axially and narrowing the penetration hole.

For Types 5-11, once the penetration depth reaches 26-27 mm, the penetration diameter remains almost constant at approximately 38 mm. This simultaneous plateau in both depth and diameter signals a limit in the energy-transfer process: after the liner collapses completely, additional impulse does not increase axial kinetic energy and is instead dispersed laterally.

Table 8. EFP penetration process for with different explosive charge length.

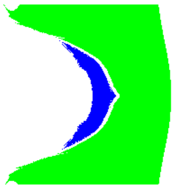			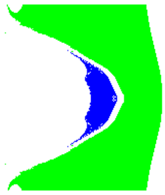
Type 1 *b*= 41 mm; d_h = 22 mm	**Type 2** *b*=40mm; d_h = 23 mm	**Type 3** *b*=40 mm; d_h = 24 mm	**Type 4** *b*=39 mm; d_h =25 mm
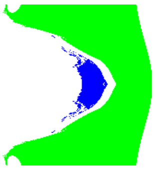			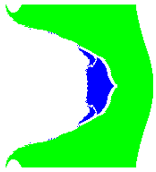
Type 5 *b*=38 mm; d_h = 26 mm	**Type 6** *b*= 38 mm; d_h = 27 mm	**Type 7** *b*= 38 mm; d_h = 27 mm	**Type 8** *b*=38 mm; d_h = 27 mm
	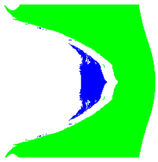		
Type 9 *b*=38 mm; d_h =27 mm	**Type 10** *b* = 38 mm; d_h =27 mm	**Type 11** *b*= 38 mm; d_h =27 mm	

The experimental test with l/d=1.2 measured an average penetration diameter of 37.7 mm (range 36-40 mm), with a deviation from the simulation of less than 5.7%. This confirms that the numerical model accurately captures the trend of decreasing hole diameter as the explosive length increases.

Overall, although the penetration depth rises sharply when *l*/d increases from 0.7*d* to roughly 1.2-1.4*d*, the penetration diameter declines and stabilises around 38 mm for *l/d* ≥1.1. This indicates that the projectile becomes more slender and that energy is used more efficiently within the optimal range of 1.2-1.4*d*. Beyond this threshold, velocity, penetration depth, and penetration diameter all reach a plateau; thus, adding further explosive mass yields no benefit and may even reduce the structural integrity of the EFP.

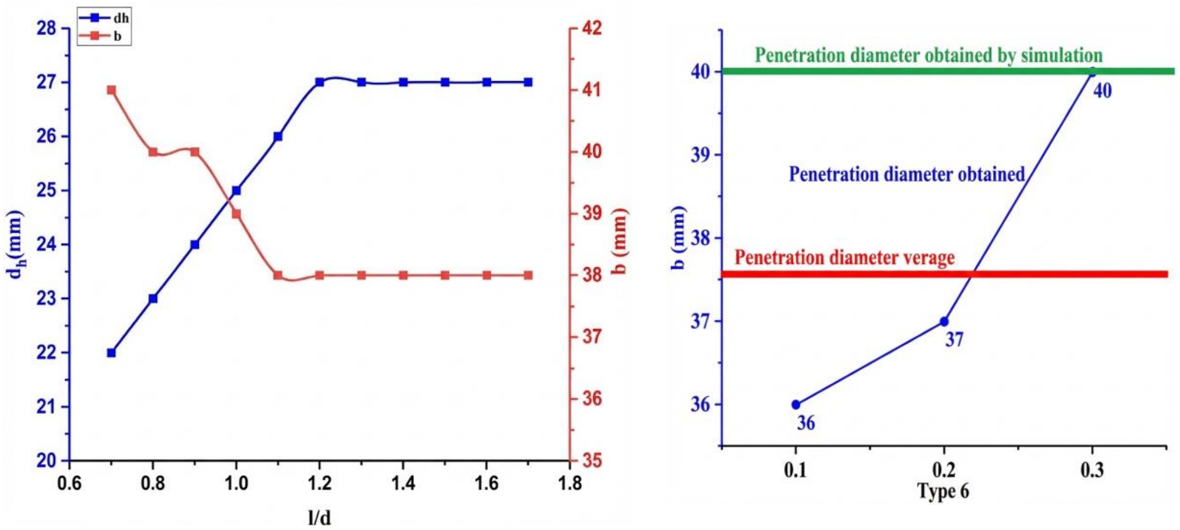

Fig. 8. Diameter and depth of EFP obtained by simulation and experiments.

These findings suggest a fundamental limit in the energy transfer mechanism between the explosive charge and the liner. In the early configurations, increasing the charge length supplies additional detonation energy that is effectively absorbed by the liner, resulting in more efficient projectile formation. However, once the liner undergoes complete deformation and optimal acceleration, any surplus energy can no longer be converted into forward momentum. Instead, this excess energy is likely dissipated through lateral expansion, shock wave dispersion, or turbulence within the cavity. In some cases, it may even destabilise the projectile formation process, leading to structural fragmentation or shape deformation. Therefore, exceeding the optimal charge length offers no performance gain and may degrade EFP structural integrity.

The optimal charge length was determined to lie between 1.2 and 1.4 times the liner diameter, corresponding to configurations Type 6 through Type 8. Within this range, the EFP achieves maximum performance in terms of both velocity and penetration depth without the drawbacks of excessive charge weight. Exceeding this range leads to diminished energy efficiency and unnecessary increases in mass, which may reduce the effectiveness of the warhead system in operational environments. Additionally, optimising the charge-to-liner diameter ratio provides opportunities to reduce warhead size and weight, allowing the integration of supplementary technologies such as precision guidance systems, multifunctional fuzes, or payload diversification.

5. Conclusions

This study employed a combination of numerical simulations and experimental tests to analyse the impact of explosive charge length on the formation and terminal behaviour of explosively formed projectiles. Eleven numerical configurations ranging from 0.7*d* to 1.7*d*, along with one experimental test at *l*/*d*=1.2, were investigated. The findings are summarised as follows:

- Projectile velocity and penetration depth increase substantially as charge length grows from 0.7d to approximately 1.4d. The most effective range for charge length is 1.2*d*-1.4*d*, which provides an optimal balance between axial acceleration, liner deformation, and energy transfer efficiency.
- Beyond *l*/*d*≈1.4 (Type 8), further increases in explosive length produce negligible improvements in performance parameters. The velocity remains

constant (~2157 m/s), penetration depth stabilises around 27 mm, and penetration diameter levels off at ~38 mm, indicating a clear performance plateau.

- The observed saturation is explained by limits in energy transfer: once the liner completes collapse and axial hydrodynamic coupling weakens, surplus explosive energy is inefficiently converted (e.g., diverted to lateral expansion and shock dispersion), and added charge no longer increases the projectile's kinetic energy.
- The experimental test at l/d=1.2 showed good agreement with simulation results. The maximum deviation in EFP velocity was less than 2.2%, while the difference in penetration diameter remained below 5.7%. These small deviations indicate that the proposed numerical simulation model agrees well with the experimental results. The optimal design range for charge length lies between 1.2d and 1.4d, ensuring maximum effectiveness while minimising unnecessary mass and material cost.

These findings establish a practical framework for EFP warhead design and optimisation. Future work should further validate the numerical predictions experimentally and investigate additional factors such as liner geometry, casing confinement, and multi-material configurations to improve system reliability and adaptability.

CRediT author statement

Hong Quan Pham: Supervision, Conceptualisation, Methodology, Writing, Reviewing; Van Minh Do: Reviewing, Methodology; Dinh Thanh Tran: Reviewing and Editing.

ACKNOWLEDGEMENTS

The authors would like to thank Le Quy Don Technical University for providing the facilities and research conditions that supported the completion of this study.

COMPETING INTEREST

The authors declare that there is no conflict of interest regarding the publication of this article.

REFERENCES

[1] S.G. Andreev, A.V. Babkin, F.A. Baum, et al. (2004), *Physics of Explosion*, edited by L.P. Orlenko, Moscow: Fizmatlit, ISBN: 5-9221-0218-6 (in Russian).

[2] L.P. Orlenko, *Physics of Explosion and Impact*, Moscow: Fizmatlit 2008, ISBN 978-5-9221-0891-1 (in Russian).

[3] J. Wu, J. Liu, Y. Du (2007), "Experimental and numerical study on the flight and penetration properties of explosively-formed projectile", *International Journal of Impact Engineering*, **34(7)**, pp.1147-1162, DOI: 10.1016/j.ijimpeng.2006.06.007.

[4] D.V. Minh, T.D. Thanh, B.X. Son, et al. (2025), *Influence of Liner Curvature Radiuses on the Formation Process and Penetration Capability of Explosively Formed Projectile*, Paper presented at the 2025 International conference on Military technologies (ICMT).

[5] H.Q. Pham, V.M. Do, D.T. Tran, et al. (2025), "Experimental and numerical study on the influence of liner height on explosively formed rrojectiles", *Journal of Advances in Military Technology*, **20(1)**, pp.211-225, DOI: 10.3849/aimt.01961.

[6] O. Jeremić, M. Milinović, M. Marković, et al. (2017), "Analytical and numerical method of velocity fields for the explosively formed projectiles, *FME Transactions*, **45(1)**, pp.38-44, DOI: 10.5937/fmet1701038J.

[7] H. Couque, R. Boulanger (2007), *EFP Simulations with Johnson-Cook Models*, 23rd International Symposium on ballistics, Tarragona, Spain.

[8] H. Couque, R. Boulanger, F. Bornet (2006), "A modified Johnson-Cook model for strain rates ranging from 103 to 105 s-1", *Journal de Physique IV (Proceedings)*, **134**, pp.87-93, EDP sciences, DOI: 10.1051/jp4:2006134015.

[9] G. Hussain, A. Hameed, J. Hetherington, et al. (2013), "Hydrocode simulation with modified Johnson-Cook model and experimental analysis of explosively formed projectiles", *Journal of Energetic Materials*, **31(2)**, pp.143-155, DOI: 10.1080/07370652.2011.606453.

[10] W. Li, X. Wang, W. Li, et al. (2012), Research on the optimum length-diameter ratio of the charge of a multimode warhead, *Shock Waves*, **22**, pp.265-274, DOI: 10.1007/s00193-012-0365-z.

[11] S. M. Zakir, L. Yulong, A. Sohail, et al. (2018), *Numerical Study on the Optimum Design of Explosively Formed Projectile*, 15th International Bhurban Conference on Applied Sciences and Technology (IBCAST), Islamabad, Pakistan, pp.128-133, DOI: 10.1109/IBCAST.2018.8312213.

[12] M. Petrudi, A. Vahedi, K. Rahmani, et al. (2020), "Numerical and analytical simulation of ballistic projectile penetration due to high velocity impact on ceramic target", *Fracture and Structural Integrity*, **14(54)**, pp.226-248, DOI:10.3221/IGF-ESIS.54.17.

[13] M. Rahmani, A.M. Petrudi (2020), "Experimental and numerical optimization study of shock wave damping in aluminum panel sandwich,

Fracture and Structural Integrity, **15(55)**, pp.88-109, DOI:10.3221/IGF-ESIS.55.07.

[14] G.R. Johnson, W.H. Cook (1985), "Fracture characteristics of three metals subjected to various strains, strain rates, temperatures and pressures", *Engineering Fracture Mechanics*, **21(1)**, pp.31-48, DOI: 10.1016/0013-7944(85)90052-9.

[15] ANSYS Autodyn User's Manual [online] (2021), https://www.scribd.com/document/453341462/ANSYS-Autodyn-Users-Manual-pdf, accessed 12 October 2025.

[16] M.R. Vaziri, M. Salimi, M.A. Mashayekhi (2010), "A new Calibration method for ductile fracture models as Chip separation criteria in machining", *Simulation Modelling Practice and Theory*, **18(9)**, pp.1286-1296, DOI: 10.1016/j.simpat.2010.05.003.

[17] W.P. Walters, J.A. Zukas (1989), Fundamentals of Shaped Charges, John Wiley & Sons.

[18] Y.B. Li, J.X. Wang, Z.T. Liu, et al. (2023), "Orthogonal optimization design and experiments on explosively formed projectiles with fins", *International Journal of Impact Engineering*, **173(3),** DOI: 10.1016/j.ijimpeng.2022.104462. (Cho thêm số trang)

[19] C. Kong, Y. Li, Y. Jin, et al. (2024), "Analysis of the influence of charge liner on the penetration effect of shaped charge jet assisted window sidetracking", *Geoenergy Science and Engineering*, **243**, DOI: 10.1016/j.geoen.2024.213300.